# Topological nodal semimetals

A. A. Burkov,[1] M. D. Hook,[1] and Leon Balents[2]
[1]*Department of Physics and Astronomy, University of Waterloo, Waterloo, Ontario, Canada N2L 3G1*
[2]*Kavli Institute for Theoretical Physics, University of California, Santa Barbara, California 93106, USA*
(Received 7 October 2011; revised manuscript received 6 December 2011; published 20 December 2011)

We present a study of "nodal-semimetal" phases in which nondegenerate conduction and valence bands touch at points (the "Weyl semimetal") or lines (the "line-node semimetal") in three-dimensional momentum space. We discuss a general approach to such states by perturbation of the critical point between a normal insulator (NI) and a topological insulator (TI), breaking either time-reversal (TR) or inversion symmetry. We give an explicit model realization of both types of states in a NI-TI superlattice structure with broken TR symmetry. Both the Weyl and the line-node semimetals are characterized by topologically protected surface states, although in the line-node case, some additional symmetries must be imposed to retain this topological protection. The edge states have the form of "Fermi arcs" in the case of the Weyl semimetal: these are chiral gapless edge states, which exist in a finite region in momentum space, determined by the momentum-space separation of the bulk Weyl nodes. The chiral character of the edge states leads to a finite Hall conductivity. In contrast, the edge states of the line-node semimetal are "flat bands": these states are approximately dispersionless in a subset of the two-dimensional edge Brillouin zone, given by the projection of the line node onto the plane of the edge. We discuss unusual transport properties of the nodal semimetals and, in particular, point out quantum critical-like scaling of the dc and optical conductivities of the Weyl semimetal and similarities to the conductivity of graphene in the line-node case.

DOI: 10.1103/PhysRevB.84.235126 PACS number(s): 71.90.+q, 75.47.−m, 03.65.Vf, 73.43.−f

## I. INTRODUCTION

The study of systems, distinguished by topology rather than symmetry, is an increasingly important theme in modern condensed matter physics. This paradigm shift has gained more momentum recently, with the discovery of the time-reversal (TR) invariant topological insulator (TI).[1–5] Apart from reinvigorating the interest in topological phenomena in solids generally, this discovery has drawn particular attention to the momentum-space topology of the electronic band structure of solid crystalline materials, or, in a more general context, to the momentum-space topology of fermionic ground states. The most common view of topologically nontrivial electronic phases is that these are states of matter, which are *insulators* in the bulk, yet have *metallic* edge or surface states, which result from the nontrivial momentum-space topology of the bulk band structure. The gap in the bulk electronic spectrum is what makes the topological ground state insensitive to small perturbations and protects (perhaps in combination with a discrete symmetry, such as TR) the metallic surface states. The appearance of such a robust metallic surface state in a bulk insulator is the main experimentally observable manifestation of topological order. This, however, is an oversimplified view. Very recent work has shown that certain special types of *gapless* band structures can in fact also be topologically nontrivial and give rise to robust gapless surface states.[6–12] Gapless topologically nontrivial band structures are characterized by the presence of point or line nodes, i.e. points or lines in the three-dimensional (3D) momentum space, at which two distinct bands touch each other accidentally. While such accidental band touchings have been known to exist and studied since the early days of the band theory of solids,[13] only much more recently have their nontrivial topological properties been noticed and their significance appreciated, starting, in particular, with the pioneering work of Volovik.[14,15]

Topological properties of the accidental band-touching nodes depend crucially on their co-dimension.[16] The point nodes, which have an odd co-dimension $3 = 3 - 0$, are the most robust variety. The band structure near such point nodes is described by a massless two-component Dirac (Weyl) Hamiltonian and is topologically equivalent to a hedgehog in momentum space.[14] The only way to eliminate such a momentum-space hedgehog is to annihilate it with an antihedgehog, i.e., Dirac point of opposite chirality. The theorem of Nielsen and Ninomiya[17] guarantees that Weyl nodes always occur in pairs of opposite chirality. Such pairs are topologically stable if the opposite-chirality partners are separated in momentum space, thus precluding their mutual annihilation. When both TR and inversion symmetry are present, however, energy bands are twofold degenerate at *all momenta*, and nontrivial contact is between *pairs* of bands. This has vanishing probability at generic points in momentum space, and occurs only by tuning one parameter at special time-reversal-invariant momenta. In the latter case, the four bands crossing can be viewed as a pair of opposite chirality Weyl nodes, which occur at the same point in momentum space, and are thus not stable, hence, the need for a tuning parameter. The separation of the two Weyl nodes in momentum space is achieved by breaking TR (Refs. 6 and 9) or inversion symmetry.[18] The resulting topological *Weyl semimetal* phase can then be shown to possess chiral edge states[6,8,9] (this is the only known example of a state with topological chiral edge states, which is intrinsically three dimensional) and a nonzero Hall conductivity, proportional to the separation of the Dirac nodes in momentum space.[8,9,19]

A line node has an even co-dimension $2 = 3 - 1$ and does not possess the absolute topological stability of a point node (this even-odd dichotomy is an example of Bott periodicity and can be understood within $K$ theory[16]). However, imposing certain discrete symmetries can stabilize line nodes, i.e., they may be stable with respect to all perturbations, not

 

violating a specific discrete symmetry.[7,20] As for point band touching, imposition of both TR and inversion symmetries is too restrictive for line touchings to occur. Thus, we consider here the case where TR is broken. However, the role of symmetry in the case of the line nodes is more complex than for Weyl nodes, and we will see that, while the line contact between bands can be stabilized, this requires a delicate, but physically achievable, combination of discrete symmetries (other than TR). Moreover, the conditions, which stabilize a line contact between two bands, are distinct from those that force this line contact to have constant energy (and are in general insufficient to guarantee constant energy). Thus, we will argue that, by physical symmetries, a line node can not be stabilized at the Fermi level. Interestingly, even a line contact, which is not at constant energy (which we will continue to call a line node although it is a slight abuse of terminology in this case), has topological properties and can be related to the surface spectrum. The distinguishing characteristic of these surface states is that they exist inside the "direct gap" between conduction and valence bands in a finite area in the 2D surface Brillouin zone (BZ), the boundary of which is determined by the projection of the bulk nodal line onto the plane of the surface. In the simplest models, which may be a reasonable approximation in some cases, these surface states are entirely dispersionless, i.e., form a "topological" flat band.[7]

In this paper, we discuss a particularly simple realization of both a Weyl and a line-node semimetal phase, which obtains in a multilayer heterostructure material, composed of alternating layers of a TI and a normal insulator (NI) material.[9] This can be understood as a simple means of constructing an underlying four-component Dirac point with both TR and inversion symmetry, describing the (unstable) critical point between a bulk NI and TI phase. Then, by a judicious choice of TR-breaking perturbation, we can realize both stable nodal phases (the alternative case, in which inversion symmetry is broken, has recently been discussed in Ref. 12). Here, we imagine doping with magnetic impurities, which are presumed to ferromagnetically align, but applying an external magnetic field will also serve, although this introduces some changes in low-energy properties due to the influence of the orbital component of the field. We provide a characterization of the edge states in the two topological semimetal phases and also discuss their transport and optical properties, which are unusual and should be a focus for experimental studies. Our results for the transport and optical properties of the Weyl semimetal apply equally well to proposed bulk realizations of the state, such as in pyrochlore iridates.[6]

The paper is organized as follows. In Sec. II, we discuss the general theory of perturbed four-component Dirac points, and classify the perturbations, which give rise to point nodes, line nodes, and Fermi-surface phases. These results may apply very generally, and allow design of any desired nodal state, once a physical meaning, appropriate to a specific system, is given to each of the Dirac matrices. In Sec. III, we review the point-node, or Weyl, semimetal, discussed previously in Ref. 9 in this context, and discuss the effects of an orbital magnetic field on this state. In Sec. IV, we give a detailed discussion of the line-node semimetal, including its unusual "flat-band" surface states and effects of an orbital field. Section V discusses the conductivity of both the Weyl and line-node states. We conclude in Sec. VI with a brief summary and discussion of our results.

## II. GENERAL THEORY: PERTURBED DIRAC POINTS

In this section, we consider generally how semimetallic phases may emerge from perturbations of a system close to a TI to NI transition in a nearly time-reversal and inversion-symmetric system. The result is that point-node, line-node, and metallic Fermi-surface states are possible, depending upon the nature of the perturbation.

### A. Dirac equation and matrices

When both TR and inversion (I) symmetry are present, a direct NI-TI transition is possible by the formation of a massless $3+1$ dimensional *four-component* Dirac fermion at the critical point.[18] This occurs at a time-reversal-invariant momentum, which for simplicity we take to be at the $\Gamma$ point $\mathbf{k}=0$. The $k\cdot p$ expansion about the $\Gamma$ point then generically takes the form

$$H_0 = \sum_{a=1}^{3} k_a \gamma_a + m\gamma_4, \tag{1}$$

where $\gamma_\mu$ $(\mu = 1,\ldots,5)$ are the five $4\times 4$ Dirac matrices in an appropriate basis. We have rescaled coordinates to set the Dirac velocity to unity for simplicity. Since the momentum components $k_a$ are odd under both TR and I, $\gamma_1,\gamma_2$, and $\gamma_3$ must also be odd under both TR and I, while $\gamma_4$ is even under both. Then, since $\gamma_5$ may be obtained as the product of the four other gamma matrices, it is odd under both TR and I. The full space of Hermitian $4\times 4$ Hamiltonians is spanned by including the identity and another 10 matrices $\gamma_{ab} = -\frac{i}{2}[\gamma_a,\gamma_b]$ with $a<b$. One can deduce their transformation properties from those of the $\gamma_\mu$. The gamma matrices can be separated into three vectors $\mathbf{b},\mathbf{b}',\mathbf{p}$ and one scalar $\varepsilon$, with transformation properties given in Table I. When both TR and I symmetry are preserved, all 10 of these matrices are prohibited from entering the Hamiltonian by symmetry. Only the mass $m$ is allowed, and there is thus a single tuning parameter to access the massless Dirac point, which separates the TI and NI phases.

### B. TR-breaking perturbations

Let us now consider what happens to this critical point when either TR or I symmetry is relaxed. First, consider relaxing TR, but preserving I. In this case, the terms $\mathbf{b}$ and $\mathbf{b}'$ may be added, and the most general Hamiltonian, which involves constant coefficients perturbing the Dirac point, is

$$H_1 = H_0 + \mathbf{u}\cdot\mathbf{b} + \mathbf{v}\cdot\mathbf{b}'. \tag{2}$$

TABLE I. Transformation properties of Dirac operators.

| Operator | TR | I |
|---|---|---|
| $\mathbf{b}=(\gamma_{23},\gamma_{13},\gamma_{12})$ | $-1$ | $+1$ |
| $\mathbf{p}=(\gamma_{14},\gamma_{24},\gamma_{34})$ | $+1$ | $-1$ |
| $\mathbf{b}'=(\gamma_{15},\gamma_{25},\gamma_{35})$ | $-1$ | $+1$ |
| $\varepsilon=\gamma_{45}$ | $+1$ | $-1$ |

In general, this is too difficult to diagonalize analytically. For several simple cases, however, it is possible.

#### *1.* **b** *perturbation*

For $\mathbf{v}=0$, by an $O(3)$ rotation, we may choose the Hamiltonian in the form $H_1 = H_0 + ub_1$. This gives the spectrum

$$\epsilon_1(v=0) = \pm\sqrt{\left(\sqrt{m^2+k_1^2}\pm u\right)^2 + k_2^2 + k_3^2}. \tag{3}$$

This gives two stable Weyl nodes with $\epsilon_1 = 0$ when $|u| > m$, with $k_1 = \pm\sqrt{u^2-m^2}$ and $k_2 = k_3 = 0$.

#### *2.* **b′** *perturbation*

Next, consider the case $\mathbf{u}=0$. In this case, by a similar rotation, we have $H_1 = H_0 + vb_1'$, and

$$\epsilon_1(u=0) = \pm\sqrt{\left(\sqrt{m^2+k_2^2+k_3^2}\pm v\right)^2 + k_1^2}. \tag{4}$$

In this case, when $|v| > m$, there are two bands whose energies touch *along a circle*, defined by $k_2^2 + k_3^2 = u^2 - m^2$, $k_1 = 0$.

#### *3.* $\mathbf{u}\cdot\mathbf{v}=0$ *perturbation*

When both **u** and **v** are nonzero, the spectrum depends upon their relative angle. When $\mathbf{u}\cdot\mathbf{v}=0$, it can still be diagonalized analytically. Taking $\mathbf{u} = (u,0,0), \mathbf{v} = (0,v,0)$,

$$\epsilon_1(\mathbf{u}\cdot\mathbf{v}=0) = \pm\Big[u^2+v^2+m^2+k^2 \pm 2\sqrt{(u^2+v^2)\left(m^2+k_1^2\right)+v^2k_3^2}\Big]^{1/2}. \tag{5}$$

From Eq. (5), one finds that when $u^2+v^2 > m^2$, there are two Weyl nodes at $k_2 = k_3 = 0, k_1 = \pm\sqrt{u^2+v^2-m^2}$, and when $u^2+v^2 < m^2$, there is a full gap.

#### *4.* $\mathbf{u}\parallel\mathbf{v}$ *perturbation*

For $\mathbf{u}\cdot\mathbf{v}\neq 0$, in general, $H_1$ can not be diagonalized analytically. An exception is the case $m=0$ and $\mathbf{u}\parallel\mathbf{v}$, in which case we can take, e.g., $\mathbf{u} = (u,0,0)$ and $\mathbf{v} = (v,0,0)$ by an $O(3)$ rotation, and the spectrum is

$$\epsilon_1(m=0) = \pm\Big[u^2+v^2+k^2 \pm 2\sqrt{u^2v^2+u^2k_1^2+v^2\left(k_2^2+k_3^2\right)}\Big]^{1/2}. \tag{6}$$

From Eq. (6), if $|u| > |v|$, one has two Weyl points at $k_1 = \pm\sqrt{u^2-v^2}$, $k_2 = k_3 = 0$, while for $|u| < |v|$, there is a ring node at $k_1 = 0$, $k_2^2 + k_3^2 = v^2 - u^2$. While we can no longer find the spectrum analytically when $m \neq 0$, in this case, we find numerically that the response to such a mass is distinct from the situations above. For small $m \neq 0$, the point and line nodes expand into Fermi surfaces: small pockets for $|u| > |v|$ and a torus for $|u| < |v|$. As $m$ is increased, these surfaces evolve and eventually shrink to a point at some threshold $m^*$, above which there is again a gap. Thus, in this case, neither point nor ring nodal states are stable, and instead the NI-TI transition is converted to an intermediate metallic state.

### C. I-breaking perturbations

If inversion symmetry is broken, but time reversal is preserved, the most general Hamiltonian with constant coefficients is of the form

$$H_2 = H_0 + \mathbf{w}\cdot\mathbf{p} + \lambda\varepsilon. \tag{7}$$

Without loss of generality, we can use an $O(3)$ rotation to choose $\mathbf{w} = (w,0,0)$, and the resulting Hamiltonian can be diagonalized to obtain

$$\epsilon_2 = \pm\Big[m^2+w^2+\lambda^2+k^2 \pm 2\sqrt{\lambda^2k_1^2+(w^2+\lambda^2)\left(k_2^2+k_3^2\right)}\Big]^{1/2}. \tag{8}$$

Here, the spectrum is fully gapped whenever $m \neq 0$. For $m=0$, there is a gapless nodal line located at $k_1 = 0$, $k_2^2 + k_3^2 = w^2 + \lambda^2$. Thus, at this level of approximation, there remains a direct NI-TI transition when $m=0$, but with a critical nodal line formed at the transition. In fact, this is an artifact of the approximation we have made, that the coefficients $m,\lambda,w$ are momentum independent. As shown in Ref. 12, when proper momentum dependence is included, this transition point broadens into a Weyl semimetal phase, with a minimum of four nodal points.

## III. POINT-NODE (WEYL) SEMIMETAL IN A TI MULTILAYER

### A. Model and connection to Dirac equation

In the previous section, we observed that a point-node state could be generated by certain time-reversal-symmetry breaking perturbations of the TI-NI Dirac critical point (e.g., Sec. II B 1). Here, we discuss the specific case of this mechanism in a model of a TI multilayer heterostructure, introduced by two of us in Ref. 9:

$$H = \sum_{\mathbf{k}_\perp,ij}\Big[v_F\tau^z(\hat{z}\times\boldsymbol{\sigma})\cdot\mathbf{k}_\perp\delta_{i,j} + \Delta_S\tau^x\delta_{i,j} + \frac{1}{2}\Delta_D\tau^+\delta_{j,i+1} + \frac{1}{2}\Delta_D\tau^-\delta_{j,i-1}\Big]c^\dagger_{\mathbf{k}_\perp i}c_{\mathbf{k}_\perp j}. \tag{9}$$

Here, $i,j$ label individual TI layers, separated by NI spacers, $\Delta_S$ is the tunneling matrix element between the top and bottom surfaces within the same TI layer, $\Delta_D$ is the tunneling matrix element between the top and bottom surfaces of nearest-neighbor TI layers, and $\mathbf{k}_\perp$ is the momentum in the 2D surface BZ of each TI layer. Without loss of generality, we will assume that $\Delta_S, \Delta_D > 0$. Such a multilayer structure exhibits a critical point between a strong 3D TI, when $\Delta_D > \Delta_S$ and an ordinary 3D insulator when $\Delta_S > \Delta_D$. The critical point $\Delta_S = \Delta_D$ realizes the four-component Dirac fermion, which is the starting point of the previous section. It occurs here when the gap vanishes at a single point in the 3D BZ $k_x = k_y = 0, k_z = \pi/d$, where $d$ is the superlattice period of the multilayer. The momentum-space Hamiltonian, expanded to leading nontrivial order near this point, is given by

$$\mathcal{H}(\mathbf{k}) = v_F\tau^z(\hat{z}\times\sigma)\cdot\mathbf{k} + \tilde{v}_F\tau^y k_z, \tag{10}$$

where $\tilde{v}_F = d\sqrt{\Delta_S\Delta_D}$. This is the Hamiltonian of a four-component massless Dirac fermion, equivalent to Eq. (1) in

Sec. II, after a rescaling of coordinates $k_x \to k_x/v_F$, $k_y \to k_y/v_F, k_z \to k_z/\tilde{v}_F$. We can identify from it a specific physical realization of the first three gamma matrices

$$\gamma_1 = -\tau^z\sigma^y, \quad \gamma_2 = \tau^z\sigma^x, \quad \gamma_3 = \tau^y. \tag{11}$$

A small deviation from criticality $m \propto \Delta_S - \Delta_D$ introduces a term proportional to $\tau^x$ (to zeroth order in the small momentum $k_x$), which identifies the remaining two gamma matrices

$$\gamma_4 = \tau^x, \quad \gamma_5 = \tau^z\sigma^z, \tag{12}$$

where $\gamma_5 = \gamma_1\gamma_2\gamma_3\gamma_4$ was used to determine the last gamma matrix. It is now indeed clear that $\gamma_5$ is odd under both time reversal (because it is proportional to spin $\sigma^z$) and inversion (it is odd under layer exchange $\tau^z \to -\tau^z$), as argued on general grounds in the previous section.

From that general analysis, we can view the critical Dirac state as the "parent" state of the topologically stable nodal semimetal phases, which we will consider below. The simplest and most robust such phase is the Weyl semimetal, which we consider first. We saw in Sec. II B 1 that the vector TR-symmetry-breaking perturbation **b** robustly splits the Dirac point into two Weyl points along the axis, parallel to **b**. Splitting the nodes along the $z$ axis therefore is accomplished, from Table I, by adding a term proportional to $b^z = \gamma_{12} = \sigma^z$, using Eq. (11). This is precisely the spin-splitting term considered by two of us in Ref. 9. After a canonical transformation

$$\sigma^{\pm} \to \tau^z\sigma^{\pm}, \quad \tau^{\pm} \to \sigma^z\tau^{\pm}, \tag{13}$$

the momentum-space Hamiltonian of the multilayer can be written in a block-diagonal form, with two independent $2 \times 2$ blocks:

$$\mathcal{H}(\mathbf{k}) = v_F k_y \sigma^x - v_F k_x \sigma^y + m_{\pm}(k_z)\sigma^z, \tag{14}$$

where $m_{\pm}(k_z) = b \pm \Delta(k_z)$, $b$ is the coefficient of the $b^z$ term (magnitude of the spin slitting), and

$$\Delta(k_z) = \sqrt{\Delta_S^2 + \Delta_D^2 + 2\Delta_S\Delta_D\cos(k_z d)}. \tag{15}$$

Taking $b > 0$, the $m_+$ mass is always nonzero, corresponding to a pair of fully gapped bands. The $m_-$ mass, on the other hand, changes sign at $k_z = \pi/d \pm k_0$, where

$$k_0 = \frac{1}{d}\arccos\left\{1 - [b^2 - (\Delta_S - \Delta_D)^2]/2\Delta_S\Delta_D\right\}. \tag{16}$$

The two points, where $m_-$ vanishes, correspond to the two Weyl fermions, separated in momentum space. The Weyl semimetal phase exists as long as

$$b_{c1}^2 = (\Delta_S - \Delta_D)^2 < b^2 < b_{c2}^2 = (\Delta_S + \Delta_D)^2. \tag{17}$$

As discussed in Ref. 9, the Weyl semimetal is characterized by a finite Hall conductivity, proportional to the separation between the Dirac nodes

$$\sigma_{xy} = \frac{e^2 k_0}{\pi h}, \tag{18}$$

and chiral edge states, which exist only in a finite subset $\pi/d - k_0 < k_z < \pi/d + k_0$ of the 2D BZ of any sample surface, not normal to the $z$ axis. For more details on this, we refer the reader to Ref. 9.

### B. Effect of orbital field

The realization of a Weyl semimetal, which we have described above, requires doping the TI layers with magnetic impurities. This is needed to produce the spin splitting $b$, which breaks TR symmetry and splits the massive Dirac fermion into two massless Weyl fermions. In practice, it is easier to break TR by simply applying an external magnetic field instead of doping the multilayer material with magnetic impurities. In this section, we will explore this route in some detail.

Let us assume that an external magnetic field of magnitude $B$ is applied along the $z$ axis, i.e., the growth direction of the multilayer. The Hamiltonian is given by

$$\mathcal{H} = v_F\tau^z(\hat{z} \times \boldsymbol{\sigma}) \cdot \left(-i\nabla + \frac{e}{c}\mathbf{A}\right) + \frac{g\mu_B}{2}B\sigma^z + \hat{\Delta}, \tag{19}$$

where

$$\hat{\Delta} = \Delta_S\tau^x\delta_{i,j} + \frac{\Delta_D}{2}(\tau^+\delta_{j,i+1} + \tau^-\delta_{j,i-1}) \tag{20}$$

is the tunneling operator in real space. We choose Landau gauge for the vector potential $\mathbf{A} = xB\hat{y}$. Since the vector potential does not enter in the tunneling term $\hat{\Delta}$, it can still be partially diagonalized by Fourier transform. Then, after the canonical transformation of Eq. (13), and after diagonalizing the tunneling term, we obtain

$$\mathcal{H} = v_F(\hat{z} \times \boldsymbol{\sigma}) \cdot \left(-i\nabla + \frac{e}{c}\mathbf{A}\right) + m_{\pm}(k_z)\sigma^z, \tag{21}$$

where $m_{\pm}(k_z) = b \pm \Delta(k_z)$ and $b \equiv g\mu_B B/2$. This is identical to the problem of 2D Dirac fermions with masses $m_{\pm}(k_z)$, which depend on a parameter $k_z$, in a perpendicular magnetic field. The solution for the spectrum is well known and is given by[21–24]

$$\epsilon_{n\lambda\pm}(k_z) = \lambda\sqrt{2\omega_B^2 n + m_{\pm}^2(k_z)}, \tag{22}$$

where $\lambda = \pm$ labels the electron and holelike sets of Landau levels, $\omega_B = v_F/\ell$ is the analog of the cyclotron frequency for Dirac fermions, $\ell = \sqrt{c/eB}$ is the magnetic length (we will be using $\hbar = 1$ units throughout, restoring explicit $\hbar$ in some of the final results), and $n = 1,2,\ldots$ are non-negative integers. As is well known, the $n = 0$, i.e., the lowest Landau level (LLL), is special and needs to be considered separately. The energy of the LLL, corresponding to the mass $m_+(k_z)$, which is always positive, is given by

$$\epsilon_{0+}(k_z) = -m_+(k_z), \tag{23}$$

i.e., the 0+ level is always holelike and lies below the zero energy line for any value of the momentum $k_z$. The situation is different for the LLL of the Dirac fermion with the $m_-(k_z)$ mass. $m_-(k_z) = b - \Delta(k_z)$ changes sign from negative to positive as the momentum $k_z$ crosses the locations of the Dirac nodes $k_z = \pi/d \pm k_0$. This means that the 0 LLL is electronlike when $|k_z - \pi/d| > k_0$, while it is holelike, i.e., dips below the zero-energy line when $|k_z - \pi/d| < k_0$ or, in other words, when $k_z$ is in the interval between the Dirac nodes. This corresponds to a jump in the Hall conductivity of the corresponding fictitious system of 2D Dirac fermions, parametrized by $k_z$, from 0 to $e^2/h$. The total Hall conductivity of the multilayer is obtained by integrating the 2D Hall

conductivity between the Dirac nodes and is still given by the same expression, as in the case of the magnetic-impurity-induced spin splitting, without any orbital component of the field, i.e., $\sigma_{xy} = e^2 k_0/\pi h$. The edge states also retain their character: these are chiral topologically protected edge states, which exist in the interval $\pi/d - k_0 < k_z < \pi/d + k_0$ in the 2D edge BZ. Thus, some of the defining and most interesting properties of the Weyl semimetals can be observed by simply applying external magnetic field to a TI-NI multilayer structure, without any doping by magnetic impurities. Also, note that the magnetic field dependence of $\sigma_{xy}$, which is given by Eq. (16), since $\sigma_{xy} \sim k_0$, is quite different from what would be expected in a regular metal. Indeed, $k_0$ is a highly nonlinear function of $B$, vanishing as $\sqrt{b^2 - (\Delta_S - \Delta_D)^2}$ near the transition from the Weyl semimetal to the insulator.

Finally, we remark that recent work has suggested a magnetoconductivity, i.e., diagonal conductivity for current and electric field parallel to an applied magnetic field, for a Weyl semimetal.[25] This was argued to be a manifestation of a "quantum anomaly" for Weyl fermions. While interesting, we note that a significant effect occurs only in the ultra-quantum limit in which $\omega_B \tau \gg 1$, where $\tau$ is the scattering time. Moreover, a large conductivity, parallel to an applied magnetic field (relative to the orthogonal components) is in fact a rather generic consequence of the ultra-quantum limit, due to the quenching of kinetic energy in the transverse directions and the suppression of backscattering in the effectively one-dimensional transport regime, resulting from high field. Thus, association of this magnetoconductivity, parallel to the applied field, with Weyl physics, seems challenging experimentally.

## IV. LINE-NODE SEMIMETALS

In this section, we will describe a realization in the same physical system of a TI multilayer of a line-node semimetal: a distinct topological semimetal phase, with zeros in the spectrum, forming continuous lines in momentum space.

### A. Parallel-field-induced nodal line

We consider a TI multilayer system in the presence of a magnetic field, parallel to the layers. This can be a real external magnetic field, or, as in the previous section, an exchange field, arising from ferromagnetic ordering of magnetic impurities, introduced into the TI material. In the case of an externally applied field, we, for now, neglect the orbital effect of the field, but will discuss it in detail later. We anticipate the presence of nodal lines from the Dirac calculations in Sec. II B 2. Indeed, from Table I and Eqs. (11) and (12), an in-plane field corresponds to $x$ and $y$ components of the $\mathbf{b}'$ perturbation, which leads to a circular node in a plane containing the $z$ axis.

Let us consider this in more detail. Without loss of generality, we assume the field is applied in the $x$ direction. The momentum-space Hamiltonian is given by

$$\mathcal{H}(\mathbf{k}) = v_F \tau^z (\hat{z} \times \boldsymbol{\sigma}) \cdot \mathbf{k} + b\sigma^x + \hat{\Delta}(k_z), \tag{24}$$

where

$$\hat{\Delta}(k_z) = \Delta_S \tau^x + \tfrac{1}{2}(\Delta_D \tau^+ e^{ik_z d} + \text{H.c.}). \tag{25}$$

The corresponding band dispersion, obtained by diagonalizing Eq. (24), is given by

$$\epsilon_\pm^2(\mathbf{k}) = v_F^2 k_x^2 + \left[b \pm \sqrt{v_F^2 k_y^2 + \Delta^2(k_z)}\right]^2, \tag{26}$$

where $\Delta(k_z)$ is given by Eq. (15). The $\epsilon_-$ branch exhibits a line node in the $yz$ plane, given by the solution of the equation

$$v_F^2 k_y^2 + \Delta^2(k_z) = b^2. \tag{27}$$

As above, for concreteness, we assume that $\Delta_{S,D} > 0$. Then, the node will be centered at $k_y = 0, k_z = \pi/d$. The node exists as long as

$$b > |\Delta_S - \Delta_D|. \tag{28}$$

### B. Stability of the parallel-field-induced nodal line

#### 1. *Nodal lines in general*

While we do not expect complete stability of the nodal line, it could be stabilized if extra symmetries are imposed upon the Hamiltonian. We need to distinguish two types of stability. First, we can ask whether the line contact of conduction and valence bands is stable. Second, we can ask whether, if this is stable, the line contact is degenerate and coincides with the Fermi energy. The answer will be that the former is possible with some discrete symmetries, while the latter can not be guaranteed by any set of discrete symmetries, although it will be approximately degenerate, and perhaps to a high degree of precision, under most reasonable circumstances.

First, we discuss the question of band touching from a general point of view. Since the nodal line occurs in a system with nondegenerate bands (away from the node itself), it is sufficient to consider a two-band Hamiltonian. This in general takes the form

$$\mathcal{H}_{2b}(\mathbf{k}) = h_0(\mathbf{k}) + h_1(\mathbf{k})\sigma^x + h_2(\mathbf{k})\sigma^y + h_3(\mathbf{k})\sigma^z, \tag{29}$$

where the Pauli matrices $\boldsymbol{\sigma}$ act in the two-band space. By simple counting of the degrees of freedom and constraints, nodal lines may occur when, for instance, one of the $h_a$, for $a = 1,2,3$, vanishes for all $\mathbf{k}$. Then, as a function of $\mathbf{k}$, two parameters must be tuned to obtain band degeneracy, i.e., to make the other two $h_a$ vanish, which results in line nodes in momentum space. Note however, that even in this case, any momentum dependence of $h_0(\mathbf{k})$, which in general is not constant along the contact line, means that the line touching does not have a constant energy and therefore can not coincide with the Fermi level. In general, there are an infinite number of functions $h_0(\mathbf{k})$, consistent with any discrete symmetries, so that this requires an "infinite" degree of fine tuning. This means that a line-node semimetal, i.e., a semimetal with a linelike Fermi "surface" in 3D is nongeneric.

Nevertheless, line contacts, even with nonconstant energy, have a robustness associated with them, which can be traced to the existence of a topological invariant characterizing the line contact. For concreteness, and without loss of generality, let us take $h_1 = 0$. Then, we may form a complex order parameter $h = h_2 + ih_3$, the phase of which is well defined everywhere

except at a node. Away from the node, we define $h = |h|e^{i\theta}$, and then, since $h$ is single valued, we have

$$\oint_{\mathcal{C}} dk^{\mu}\partial_{\mu}\theta = 2\pi n, \tag{30}$$

where $n$ is an integer for any closed curve $\mathcal{C}$ in momentum space on which the bands are nondegenerate. Since this winding number is quantized, it can not change as this curve is smoothly deformed. If the curve does not contain any singularity inside it (i.e., points where $h$ vanishes: nodes), then it can be shrunk to a point and the winding number $n$ must vanish. Generically, however, a curve that encircles a nodal line has $n = \pm 1$, depending upon the sense of circulation. The nodal line can therefore be viewed as a vortex line in momentum space. So long as vanishing $h$ requires a band degeneracy, this is the case. However, if we allow the third component $h_1 \neq 0$, then $h = h_2 = h_3 = 0$ does not require a band degeneracy, and a curve with nonzero $n$ need not enclose a node.

This can be understood in a yet more general context. Specifically, the line integral in Eq. (30) can be viewed more generally as a Berry phase. Whenever the bands are nondegenerate, we can define a U(1) Berry gauge field (Berry connection) from the periodic part of the Bloch wave functions $u_{\mathbf{k}\alpha}(\mathbf{r})$, where $\alpha$ is the "spin index," associated with the Pauli matrices in Eq. (29):

$$\mathcal{A}_{\mu}(\mathbf{k}) = -\frac{i}{2}\int_{r\in \text{u.c.}}\left[u^{*}_{\mathbf{k}\alpha}(\mathbf{r})\frac{\partial}{\partial k_{\mu}}u_{\mathbf{k}\alpha}(\mathbf{r}) - \frac{\partial}{\partial k_{\mu}}u^{*}_{k\alpha}(\mathbf{r})u_{\mathbf{k}\alpha}(\mathbf{r})\right], \tag{31}$$

where the integral is taken over the unit cell of the crystal. The Berry curvature is the flux of this gauge field:

$$\mathcal{B}_{\mu}(\mathbf{k}) = \epsilon_{\mu\nu\lambda}\partial_{\nu}\mathcal{A}_{\lambda} = -i\epsilon_{\mu\nu\lambda}\int_{r\in \text{u.c.}}\frac{\partial}{\partial k_{\nu}}u^{*}_{\mathbf{k}\alpha}(\mathbf{r})\frac{\partial}{\partial k_{\lambda}}u_{\mathbf{k}\alpha}(\mathbf{r}). \tag{32}$$

Stable nodal lines occur *when the Berry curvature is generically (i.e., for nondegenerate points) vanishing*. This is because one may write the line integral as

$$\oint_{\mathcal{C}} dk^{\mu}\mathcal{A}_{\mu}(\mathbf{k}) = \int_{\mathcal{S}} dn^{\mu}\mathcal{B}_{\mu}(\mathbf{k}) \tag{33}$$

by Stokes' theorem, where $\mathcal{S}$ is a surface in reciprocal space, the boundary of which is $\mathcal{C}$. For any surface for which there is no band touching, $\mathcal{B}_{\mu} = 0$ would imply a vanishing "vorticity." Conversely, nonvanishing vorticity within $\mathcal{C}$ implies nonvanishing Berry curvature on $\mathcal{S}$. If the Berry curvature is generically zero, then this in turn requires a singularity on $\mathcal{S}$, i.e., that $\mathcal{S}$ is crossed by a nodal line. However, if there is no such requirement of vanishing Berry curvature, there need be no singularity, and the curvature may be spread out over the region of integration.

The vanishing Berry curvature condition holds in the above example because, when $h_1 = 0$, the Hamiltonian obeys $\sigma^{z}\mathcal{H}^{*}(\mathbf{k})\sigma^{z} = \mathcal{H}(\mathbf{k})$. When this condition is obeyed, the Bloch functions satisfy $u^{*}_{k\alpha} = \sigma^{z}_{\alpha\beta}u_{k\beta}$, which implies a vanishing $\mathcal{B}_{\mu}$ from Eq. (32). One can see that such a vanishing-Berry-curvature condition generally requires some discrete symmetry, involving conjugation of the Hamiltonian at a single momentum point. Without both inversion and time-reversal symmetry present, this is, in general, artificial. Nevertheless, it may be imposed in toy models, or may be approximately the case for some physical situations, such as discussed here.

#### 2. *Superlattice case*

We now return to the specific case of the nodal line, induced in the TI-NI superlattice by an in-plane field. It is instructive to reduce the Hamiltonian to a two-band form, containing just the bands involved in the line node. To do so, we first rotate the spin quantization axis by $\pi/2$ around the $y$ axis, taking $\mathcal{H} \to \tilde{\mathcal{H}}$:

$$\tilde{\mathcal{H}}(\mathbf{k}) = (b + v_F\tau^{z}k_y)\sigma^{z} + \hat{\Delta}(k_z) - v_F\tau^{z}\sigma^{y}k_x, \tag{34}$$

and then make the canonical transformation of Eq. (13), under which $\tilde{\mathcal{H}} \to \mathcal{H}'$, with

$$\mathcal{H}'(\mathbf{k}) = [b + v_F\tau^{z}k_y + \hat{\Delta}(k_z)]\sigma^{z} - v_F\sigma^{y}k_x. \tag{35}$$

The term in the square brackets is now a constant of motion and can be replaced by its eigenvalues

$$m_{\pm}(\mathbf{k}) = b \pm \sqrt{v_F^2k_y^2 + \Delta^2(k_z)}. \tag{36}$$

Then, we obtain two independent blocks of the Hamiltonian

$$\mathcal{H}'_{\pm}(\mathbf{k}) = m_{\pm}\sigma^{z} - v_Fk_x\sigma^{y}. \tag{37}$$

The low-energy block containing the node corresponds to $\mathcal{H}'_{-}$ and indeed has the form described in Sec. IV B 1. It has a symmetry $\mathcal{W}$ (for "wishful thinking"):

$$\mathcal{W}: \ \sigma^{z}[\mathcal{H}'_{\pm}(\mathbf{k})]^{*}\sigma^{z} = \mathcal{H}'_{\pm}(\mathbf{k}). \tag{38}$$

But is this symmetry physical?

Complex conjugation occurs physically only through time reversal, which we denote by $\mathcal{T}$. $\mathcal{T}$ acts on the original Hamiltonian, Eq. (24), as $\mathcal{H}(\mathbf{k}) \to \sigma^{y}\mathcal{H}^{*}(-\mathbf{k})\sigma^{y}$. It is not a symmetry due to the applied Zeeman field $b$. However, if combined with a $\pi$ rotation about the $z$ axis, $\mathcal{R}^{z}_{\pi}$, the invariance is restored. So, a physical symmetry is

$$\mathcal{T}\circ\mathcal{R}^{z}_{\pi}: \ \mathcal{H}(k_x,k_y,k_z) \to \sigma^{x}\mathcal{H}^{*}(k_x,k_y,-k_z)\sigma^{x}. \tag{39}$$

Carrying through the transformations from $\mathcal{H}(\mathbf{k})$ to $\mathcal{H}'_{\pm}(\mathbf{k})$, invariance under $\mathcal{T}\circ\mathcal{R}^{z}_{\pi}$ requires

$$\mathcal{T}\circ\mathcal{R}^{z}_{\pi}: \sigma^{z}[\mathcal{H}'_{\pm}(k_x,k_y,k_z)]^{*}\sigma^{z} = \mathcal{H}'_{\pm}(k_x,k_y,-k_z). \tag{40}$$

This is close to, but not precisely, the required condition to protect the node because it involves a sign change of $k_z$. We can attempt to reverse this sign change by imposing an additional $z \to -z$ reflection symmetry on the problem, which might naturally be associated with reflection with respect to a constant $z$ plane at the center of the TI or NI layers. However, because spin is a pseudovector, this will flip the in-plane components of the spin $\sigma^{x} \to -\sigma^{x}$, $\sigma^{y} \to -\sigma^{y}$. This does not leave the in-plane field $b\sigma^{x}$ invariant, so can not be a symmetry of Eq. (24).

Because the growth direction and applied field fully break any possible threefold or fourfold rotation axes, only some discrete $Z_2$-type symmetries remain as candidates. One possible remaining symmetry consistent with the applied field is inversion $\mathcal{I}$ through a center midway through a TI or NI

layer. Since spin is a pseudovector, this leaves $\boldsymbol{\sigma}$ invariant. Upper and lower layers of each TI layer are interchanged, and $\mathbf{k} \to -\mathbf{k}$, so this condition gives

$$\mathcal{I}: \ \mathcal{H}(\mathbf{k}) \to \tau^x \mathcal{H}(-\mathbf{k})\tau^x, \tag{41}$$

which is indeed an invariance of Eq. (24). After the changes of basis, $\mathcal{I}$ implies for Eq. (35) that

$$\mathcal{I}: \ \sigma^z\tau^x\mathcal{H}'(\mathbf{k})\tau^x\sigma^z = \mathcal{H}'(-\mathbf{k}). \tag{42}$$

Finally, after projection into the $2 \times 2$ blocks, the final condition, imposed by inversion symmetry $\mathcal{I}$, is

$$\mathcal{I}: \ \sigma^z\mathcal{H}'_{\pm}(\mathbf{k})\sigma^z = \mathcal{H}'_{\pm}(-\mathbf{k}). \tag{43}$$

Another possible symmetry is a twofold ($\pi$) rotation about the axis of the field $\mathcal{R}^x_\pi$. This acts as

$$\mathcal{R}^x_\pi: \ \mathcal{H}(k_x,k_y,k_z) \to \sigma^x\tau^x\mathcal{H}(k_x,-k_y,-k_z)\tau^x\sigma^x, \tag{44}$$

which can be verified to be a symmetry of Eq. (24). Mapping this to the rotated frame, we obtain

$$\mathcal{R}^x_\pi: \ \mathcal{H}'(k_x,k_y,k_z) \to \tau^x\mathcal{H}'(k_x,-k_y,-k_z)\tau^x. \tag{45}$$

Projecting down to the $2 \times 2$ blocks, this gives

$$\mathcal{R}^x_\pi: \ \mathcal{H}'_{\pm}(k_x,k_y,k_z) = \mathcal{H}'_{\pm}(k_x,-k_y,-k_z). \tag{46}$$

Even if invariance under all three symmetries ($\mathcal{T} \circ \mathcal{R}^z_\pi$, $\mathcal{I}$, and $\mathcal{R}^x_\pi$) is imposed, this is not equivalent to Eq. (38), and the nodal line is, at first sight, not guaranteed to be stable. In particular, a nonzero $h_1(\mathbf{k})$ (proportional to $\sigma^x$) is allowed to enter $\mathcal{H}'_-$ in Eq. (37), which could destabilize the nodal line. However, one may show that $h_1(\mathbf{k})$ must, according to these three symmetries, be an odd function, *separately* of $k_x$, $k_y$, and $k_z$. In particular, this implies that the $h_1(k_x = 0,k_y,k_z) = 0$ term vanishes on the $y$-$z$ plane, where the nodal line exists. Therefore, *the band contact along the nodal line is indeed protected* when all three symmetries are present.

We may also consider, however, the constant part of the two-band Hamiltonian $h_0(\mathbf{k})$. This is required, by the same symmetries, to be an *even* function separately of $k_x$, $k_y$, and $k_z$, and hence does not vanish nor need be a constant at $k_x = 0$. Physically, this term would arise, for example, from the always-present particle-hole asymmetry of the TI surface states. Generically, this splits the zero-energy Fermi line into a set of small electron and hole Fermi surfaces, converting the line-node state into a conventional low-carrier-density semimetal. However, the topological surface state, associated with the nodal line, survives the addition of the $h_0(\mathbf{k})$ term, although acquires a dispersion [while it is strictly dispersionless in the absence of $h_0(\mathbf{k})$].

### C. Surface states

While the line node at the Fermi energy is not generic, it may well be a good approximation, and regardless, the line band contact itself is more robust, as we have seen above. It is interesting to understand the consequences of this bulk band topology for the boundary. Indeed, Heikkilä and Volovik have shown in another context that unusual surface states are related to a nodal degeneracy.[7,20] To uncover the nontrivial surface effects of the line node, it is useful to view the Hamiltonian $\mathcal{H}(\mathbf{k})$ as describing a set of 1D systems, parametrized by momentum components $k_y$,$k_z$: $\mathcal{H}_{k_y,k_z}(k_x)$. Such a one-dimensional two-band Hamiltonian supports a topological classification, if only two of three Pauli matrices are present in it, which is the same as the condition to generically support a line node. In this case, we can define a winding number analogously to Eq. (30), but with the contour $\mathcal{C}$ taken along the periodic direction $k_x$ in reciprocal space, i.e., across the entire BZ. Thus, the same condition, which generically gives stable nodal lines, also allows such a 1D topological classification. When the 1D winding number $n$ is nonzero, then a bound state is expected at an interface between the system and another system with a different value of $n$, e.g. $n = 0$, corresponding to the vacuum. Indeed, recall the formula for the canonically transformed Hamiltonian in Eq. (37), but regarded as a 1D Hamiltonian, parametrized by $k_y$,$k_z$:

$$\mathcal{H}'_{-;k_y,k_z}(k_x) = m_-(k_y,k_z)\sigma^z - v_F\sigma^y k_x. \tag{47}$$

The mass $m_-(\mathbf{k})$ changes sign from negative to positive when

$$b = b_c(k_y,k_z) = \sqrt{v_F^2k_y^2 + \Delta^2(k_z)}. \tag{48}$$

Although this Hamiltonian is written only for small $k_x$, and hence does not describe the full 1D topology, it does describe *transitions* between different topologies, which occur when the mass $m_-$ changes sign. The 1D TI-NI transition occurs when the above condition is satisfied, so that when $m_- > 0$, one has a nontrivial 1D insulator and surface bound states, while when $m_- < 0$, the 1D insulator is trivial and no bound states are guaranteed at the surface for such $k_y$,$k_z$.

To see this explicitly, let us assume that the sample occupies the $x < 0$ half-plane with a surface at $x = 0$. To find the edge states of the 1D TI inside the nodal line, we replace $k_x \to -i\partial/\partial x$ and look for solutions of the $2 \times 2$ Dirac equation

$$\mathcal{H}'_{-;k_y,k_z}\Psi = 0 \tag{49}$$

in the following form:

$$\Psi_{k_y,k_z}(x) = i\sigma^y e^{F_{k_y,k_z}(x)}\phi, \tag{50}$$

where $\phi$ is a two-component spinor. By substituting this ansatz into the Dirac equation, we obtain

$$\left[m_-(k_y,k_z,x)\sigma^x - v_F\frac{dF}{dx}\right]\phi = 0. \tag{51}$$

Assuming $b(x \to \infty) = 0$, the solution is given by

$$\Psi_{k_y,k_z}(x) = e^{\frac{1}{v_F}\int_0^x dx' m_-(k_y,k_z,x')}|\sigma^x = -1\rangle. \tag{52}$$

This is normalizable and localized at the surface for all $b_c(k_y,k_z) < b$. The set of these zero-energy edge states forms a flat band in the surface BZ, which is dispersionless for all $k_y$,$k_z$ inside the area, enclosed by the projection of the nodal line on the surface plane. If we now add the $h_0(\mathbf{k})$ perturbation to the Hamiltonian (47), it is easy to show, using the standard quantum mechanical perturbation theory, that to leading order in $h_0$, the surface state acquires a dispersion proportional to $h_0(0,k_y,k_z)$. The full surface flat-band dispersion, calculated numerically (in the absence of the $h_0$ term), is shown in Fig. 1.

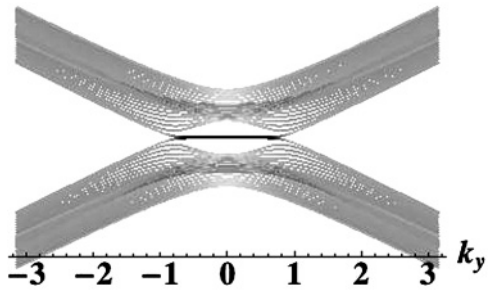


FIG. 1. The $k_z = 5\pi/6d$ section of the eigenstate spectrum for a sample of finite size in the $x$ direction with $\Delta_D/\Delta_S = 0.8$, and $b/\Delta_S = 1$. $k_y$ is in units of $\Delta_S/v_F$. The intensity of gray is a function of the degree of surface localization of a given eigenstate, measured by an inverse participation ratio of its wave function. The surface-state dispersion is black, while bulk states are lighter gray.

In the presence of $h_0(\mathbf{k})$ terms, which will give the surface state a dispersion, the remaining robust topological property of the surface state will be its termination at the projection of the nodal line to the surface BZ, as shown in Fig. 2.

As discussed above, $h_0(\mathbf{k})$ kills the bulk line node itself, transforming the line-node semimetal to a more "conventional" semimetal with a Fermi surface, containing electron and hole pockets of equal volume (at charge neutrality), as shown in Fig. 3. It is, however, distinguished from a truly conventional semimetal by the presence of the topological surface states, described above.

### D. Effect of the orbital part of the field

We have so far ignored completely the effect of the orbital part of the parallel field, which creates the line node in our system. This is justified when the parallel field is an exchange spin-splitting field, coming from the interaction with ferromagnetically ordered magnetic impurities. If the field is an externally applied magnetic field, however, a situation that is perhaps more easily realizable experimentally, the orbital effect of the field needs to be considered as in the case of the Weyl semimetal discussed above.

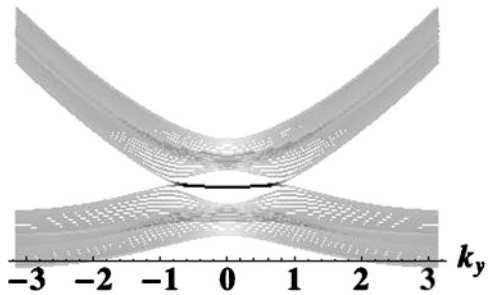


FIG. 2. The $k_z = 5\pi/6d$ section of the eigenstate spectrum for a sample of finite size in the $x$ direction with $\Delta_D/\Delta_S = 0.8$, and $b/\Delta_S = 1$ in the presence of a particle-hole asymmetry in the TI surface-state spectrum of the form $(k_x^2 + k_y^2)/2m^*$, with $1/m^* = 0.3v_F^2/\Delta_S$. $k_y$ is in units of $\Delta_S/v_F$. The surface state has acquired a dispersion due to the particle-hole asymmetry.

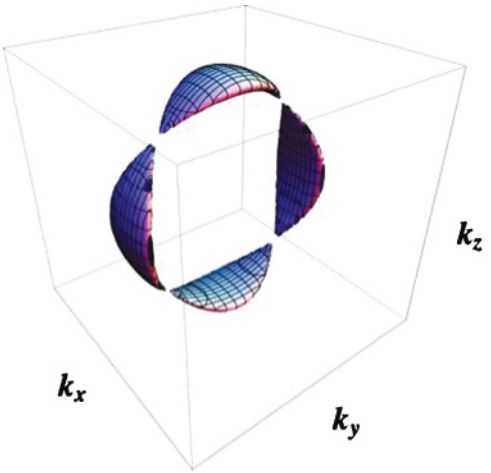


FIG. 3. (Color online) The "Fermi line" transforms into a finite-volume Fermi surface with equal-volume electron (top and bottom) and hole (left and right) pockets due to the particle-hole asymmetry of the TI surface states. Note that the line contact of the conduction and valence bands survives, although it is not a constant energy curve. This line contact threads through the middle of the chain of small Fermi surfaces, and as a consequence the topological surface state remains (see Fig. 2). The parameters here are taken to be the same as in Fig. 2.

The Hamiltonian in the presence of a magnetic field of magnitude $B$, directed along the $x$ axis, is given by

$$\mathcal{H} = v_F \tau^z (\hat{z} \times \boldsymbol{\sigma}) \cdot \left(-i\nabla + \frac{e}{c}\mathbf{A}\right) + \frac{g\mu_B}{2} B\sigma^x + \hat{\Delta}, \qquad (53)$$

where $\hat{\Delta}$ is the tunneling operator in real space, given by Eq. (20). We choose Landau gauge for the vector potential $\mathbf{A} = -zB\hat{y}$, in which case $\mathbf{A}$ does not enter in the tunneling term. We would like to point out here that the magnitude of the $g$ factor is large in typical TI materials, e.g., $g \approx 50$ in $Bi_2Se_3$, so the Zeeman term will produce a significant spin splitting at reasonable values of the magnetic field. This remark is also relevant for the Weyl semimetal in the magnetic field case, discussed above.

The general case of TI multilayer in a parallel field can only be studied numerically, as this is a Hofstadter-type problem. However, two limits can be studied analytically.

#### 1. *Limit of almost decoupled TI layers:* $\Delta_D \ll \Delta_S$

In this limit, the problem reduces to the one of a single TI layer in parallel magnetic field, already considered by two of us in Ref. 26. Neglecting the contribution of $\Delta_D$, $\Delta(k_z) = \Delta_S$ becomes independent of momentum. The nodal line in this case has the form of two straight lines, parallel to the $z$ axis, crossing the $y$ axis at $k_y = \pm k_0$, where

$$k_0 = \sqrt{\epsilon_B^2 - \Delta_S^2}. \qquad (54)$$

$\epsilon_B = v_F \kappa_B$ is the "magnetic energy," with the "magnetic wave vector" $\kappa_B$ given by

$$\kappa_B = \frac{d_{\mathrm{TI}}}{2\ell^2} - \frac{g}{4mv_F\ell^2}, \qquad (55)$$

where $d_{\rm TI}$ is the thickness of a TI layer and $\ell = \sqrt{c/eB}$ is the magnetic length. The first term in Eq. (55) comes from the orbital part of the field, while the second term comes from the Zeeman spin-splitting part. The topological surface state in this case consists of a set of $1D$ edge states of each TI layer, which are dispersionless in the $y$ direction when $-k_0 \leqslant k_y \leqslant k_0$. The surface state also does not disperse in the $z$ direction, but for the trivial reason of the absence of tunneling between individual TI layers.

#### 2. *Weak field limit*

The weak field limit applies when

$$|\Delta_S - \Delta_D| \ll \Delta_S + \Delta_D, \tag{56}$$

which implies that we can assume

$$b \ll \Delta_S + \Delta_D, \ \ell \gg d, \tag{57}$$

where we have used shorthand notation for the Zeeman spin-splitting term

$$b = \frac{g\mu_B}{2} B. \tag{58}$$

In this case, first setting the orbital part of the field to zero, we can expand $\mathcal{H}(\mathbf{k})$ in Taylor series around $k_z = \pi/d$, which is the location of the nodal-line center in the absence of the orbital component of the field. By expanding to leading order in $k_z - \pi/d$, and shifting the zero of the momentum to $k_z = \pi/d$, we obtain

$$\hat{\Delta}(k_z) \approx (\Delta_S - \Delta_D)\,\tau^x + \Delta_D d\,\tau^y k_z. \tag{59}$$

Rotating by $\pi/2$ around the $y$ axis and performing the canonical transformation of Eq. (13), the problem reduces to finding the Landau level spectrum of the following $2 \times 2$ Hamiltonian:

$$H = v_F \tau^z \pi_y + \Delta_D d\,\tau^y \pi_z + (\Delta_S - \Delta_D)\,\tau^x, \tag{60}$$

where $\boldsymbol{\pi}$ is the kinetic momentum

$$\pi_y = -i\frac{\partial}{\partial y} - \frac{z}{\ell^2}, \quad \pi_z = -i\frac{\partial}{\partial z}. \tag{61}$$

The Landau-level spectrum is easily found in the standard way by introducing ladder operators as

$$\begin{aligned} \pi_y &= \sqrt{\frac{\tilde{v}_F}{2v_F\ell^2}}(a^\dagger + a), \\ \pi_z &= -i\sqrt{\frac{v_F}{2\tilde{v}_F\ell^2}}(a^\dagger - a), \end{aligned} \tag{62}$$

where $\tilde{v}_F = d\sqrt{\Delta_S\Delta_D} \approx d\Delta_D$ has the meaning of the Fermi velocity, associated with the $z$ direction in momentum space. The resulting Landau-level spectrum, taking $\Delta_S \approx \Delta_D$, is given by

$$\epsilon_{n\pm} = \pm\sqrt{2\omega_B^2 n}, \tag{63}$$

where $\omega_B = \sqrt{v_F\tilde{v}_F}/\ell$ and $n = 0,1,2,\ldots$. The full Hamiltonian (53) can now be written as

$$\mathcal{H}_n(k_x) = \left[b \pm \sqrt{2\omega_B^2 n}\right]\sigma^z - v_F\sigma^y k_x. \tag{64}$$

By exactly the same reasoning as in Sec. IV A, we can conclude that topological zero-energy surface states appear when

$$b > \sqrt{2\omega_B^2 n}. \tag{65}$$

The surface states in the case of an externally applied parallel magnetic field will thus consist of Landau levels, which become localized at the surface of the sample normal to the applied field. In other words, the topological surface flat bands at zero field transform into surface-bound Landau levels in an applied magnetic field.

## V. CONDUCTIVITY OF THE NODAL STATES

In this section, we discuss the dc and optical conductivity of the nodal states described in the previous sections.

### A. Weyl semimetal

Here, we focus on the diagonal transport characteristics of the Weyl semimetal, namely, its optical conductivity. The simplest possible calculation of the conductivity, neglecting interactions, assuming charge neutrality, and taking into account only random point impurities, was quoted in Ref. 9, but the results were not derived in detail. Here, we give a somewhat more general discussion, and in particular show that, in fact, Coulomb interactions drastically change the behavior of the conductivity at low temperature. In particular, the result of Ref. 9 survives only at high temperature, and if the basic interaction scale, defined by the effective fine-structure constant $\alpha = e^2/\epsilon_d v_F$ (where $\epsilon_d$ is the dielectric constant) is small, $\alpha \ll 1$. In general, we will show that the frequency, doping, and temperature dependences of the conductivity of the Weyl semimetal are very unusual and can be used for experimental characterization of this phase of matter. Moreover, with interactions and charged donors taken into account, we argue that the conductivity obeys, up to logarithmic corrections, a scaling form in its dependence upon $T$, $\omega$, and donor impurity density $n_i$.

The failure of the noninteracting point impurity result is in dramatic contrast to conventional metallic systems in which elastic scattering from defects *dominates* over inelastic electron-electron processes at low temperature, which are frozen out due to phase-space restrictions. Even in the apparently close analog of 2D graphene, disorder dominates the low-energy transport rather than interactions, in striking contrast to the 3D Weyl semimetal. This difference can be explained without detailed calculations from a simple renormalization-group (RG) argument. Consider the action of the Dirac/Weyl fermion model in $d$ dimensions with both point disorder and interactions with a $1/r$ Coulomb potential:

$$\begin{aligned} S = &\int d\tau\, d^d x\, [\overline{\psi}(\partial_\tau + i\gamma_\mu\partial_\mu)\psi + V_i(x)\overline{\psi}A_i\psi] \\ &+ \int d\tau d^d x d^d x' (\overline{\psi}\psi)_{x,\tau}\frac{e^2}{2|x-x'|}(\overline{\psi}\psi)_{x',\tau}, \end{aligned} \tag{66}$$

where here $V_i(x)$ are random potentials, coupling to the fermion fields via some matrices $A_i$ (not specified), and $e$ is the electron charge. We take the quenched random potentials to have zero mean and Gaussian variance $\overline{V_i(x)V_j(x')} =$

$\Delta_{ij}\delta^{(d)}(x-x')$, reflecting short-range correlations. To keep the free Dirac/Weyl action scale invariant, we must under an RG transformation rescale length and time as $x \to bx$, $t \to bt$, and $\psi \to b^{-d/2}\psi$. Under this rescaling, we see that the Coulomb interaction term, proportional to $e^2$, is marginal in any dimension. However, the random potential $V_i(x) \to bV_i(bx)$, which implies that the disorder strength $\Delta_{ij} \to b^{2-d}\Delta_{ij}$. Thus, in the $d = 2$ case of graphene, disorder and interactions are both marginal by power counting. In fact, more careful analysis shows that interactions are marginally *irrelevant* and disorder is marginally *relevant* at the free Dirac fixed point. As a consequence of the marginally relevant disorder, a density of states is generated and the system is described at low energy by a *diffusive* fixed point. By contrast, for the $d = 3$ Dirac/Weyl fermion, interactions remain marginal (actually, marginally irrelevant, as a more detailed analysis shows[27]), but disorder becomes strongly *irrelevant* $\Delta \to \Delta/b$. Thus, in fact, the *ballistic* fixed point is stable for weak disorder in three dimensions. Moreover, since disorder is much more irrelevant than interactions at this fixed point, elastic scattering is suppressed relative to inelastic scattering, and this explains the dramatic difference from the 2D graphene case. In fact, the marginality of interactions means that many physical properties almost scale like those, expected of a fully interacting scale-invariant critical theory, with only logarithmic corrections. This simple "quantum critical" scaling is an attractive feature of the Weyl semimetal.

In the remainder of this section, we will go beyond these scaling considerations and verify their conclusions in some simple calculations. We will also extend the discussion to the physically relevant situation in which *donor impurities* are present, which extends in a simple way the quantum critical scaling due to interactions to include finite residual resistivity at $T = 0$.

#### *1. Short-range impurities for noninteracting electrons*

We first recapitulate the calculation of Ref. 9 since all details were omitted in it. We assume a model with short-range impurity scattering potential of the form

$$V(\mathbf{r}) = u_0 \sum_a \delta(\mathbf{r} - \mathbf{r}_a), \tag{67}$$

where $\mathbf{r}_a$ label the impurity positions, and also neglect electron-electron interactions. Both of these assumptions are generally quite unrealistic, both for an undoped Weyl semimetal, in which Coulomb interactions are essentially unscreened, and for a doped semimetal, where scattering from charged donors with long-range potential can be expected to dominate. However, this model will still give us useful results, which can be expected to be applicable at the neutrality point at high enough temperature such that the impurity scattering rate exceeds the scattering rate due to electron-electron interactions.

We will assume that the impurity potential is diagonal in both the spin and the pseudospin indices and will consider a single Weyl fermion in the 3D BZ with a Hamiltonian

$$\mathcal{H}(\mathbf{k}) = v_F \boldsymbol{\sigma} \cdot \mathbf{k}. \tag{68}$$

Generalization to any number of distinct Weyl fermions is trivial as they contribute additively to transport (we will assume that the impurity potential does not mix Weyl fermions at different points in the BZ).

In the first Born approximation, the impurity scattering rate is given by

$$\frac{1}{\tau(\epsilon)} = -\gamma \,\mathrm{Im} \int \frac{d^3k}{(2\pi)^3} \sum_\lambda G^R_\lambda(\epsilon,\mathbf{k}) = 2\pi\gamma g(\epsilon), \tag{69}$$

where

$$G^R_\lambda = \frac{1}{\epsilon - \lambda v_F k + i\eta} \tag{70}$$

is the retarded Green's function of the Weyl fermion, $\lambda = \pm$ labels the helicity of the positive and negative energy Dirac cones, $\gamma = u_0^2 n_i$, where $n_i$ is the impurity concentration, and the density of states $g(\epsilon)$ is given by

$$g(\epsilon) = \frac{\epsilon^2}{2\pi^2 v_F^3}. \tag{71}$$

Thus, $1/\tau(\epsilon) \sim \epsilon^2 \ll \epsilon$, which means that the conductivity can be calculated semiclassically using the Boltzmann equation. By solving the linearized Boltzmann equation with the energy-dependent momentum relaxation rate (69) in the standard way, we obtain

$$\mathrm{Re}\ \sigma_{xx}(\omega) = -\frac{e^2 v_F^2}{3} \int_{-\infty}^{\infty} d\epsilon\, g(\epsilon) \frac{dn_F(\epsilon)}{d\epsilon} \frac{1/\tau(\epsilon)}{\omega^2 + 1/\tau(\epsilon)^2}, \tag{72}$$

where $n_F$ is the Fermi distribution function at temperature $T$. By introducing dimensionless integration variable $x = \epsilon/2T$ (using $k_B = 1$ units) and restoring explicit $\hbar$, we obtain

$$\mathrm{Re}\ \sigma_{xx}(\omega) = \frac{e^2 v_F^2}{6\gamma h} \int_{-\infty}^{\infty} dx\ \frac{x^4\,\mathrm{sech}^2(x)}{x^4 + \left(h^3 v_F^3 \omega/32\pi^2\gamma T^2\right)^2}. \tag{73}$$

This gives a dc conductivity

$$\sigma_{\mathrm{dc}} = \frac{e^2 v_F^2}{3\gamma h}, \tag{74}$$

and a Drude-type peak in the optical conductivity, but with a temperature-dependent width, scaling as $T^2$. This is a very unusual property of the optical conductivity in a metal and can be used to characterize the Weyl semimetal phase experimentally.

The Drude peak also has a highly unusual shape, with a divergent first derivative. This can be obtained explicitly from Eq. (73), evaluating the integral in (73) in the limit $\omega \to 0$:

$$\mathrm{Re}\ \sigma_{xx}(\omega) \approx \frac{e^2 v_F^2}{3\gamma h}\left(1 - \frac{1}{8}\sqrt{\frac{\omega\, v_F^3 h^3}{2\,\gamma T^2}}\right). \tag{75}$$

### 2. *Donor impurities*

Now, let us consider a doped Weyl semimetal and adopt a more realistic model with Coulomb, rather than short-range, impurities, which will represent the charged donors. As is well known, the Boltzmann approach can still be used in this case, with transport time replacing the momentum relaxation time of Eq. (69):

$$\frac{1}{\tau_{\rm tr}(\epsilon)} = \pi n_i g(\epsilon) \int_0^\pi d\theta \sin(\theta) |V(q)|^2 \times [1-\cos(\theta)] \frac{1+\cos(\theta)}{2}, \quad (76)$$

where

$$V(q) = \frac{4\pi e^2}{\epsilon_d \left(q^2 + q_{\rm TF}^2\right)} \quad (77)$$

is the screened Coulomb potential with the Thomas-Fermi wave vector $q_{\rm TF}^2 = 4\pi e^2 g(\epsilon)$, $\theta$ is the scattering angle, $q = 2(\epsilon/v_F)\sin(\theta/2)$, and $n_i$ is the impurity concentration. The factor $1-\cos(\theta)$ is the standard factor, suppressing the forward-scattering contribution to the transport collision rate, while the $[1+\cos(\theta)]/2$ factor arises from the matrix elements of the impurity potential with respect to the eigenstates of the Weyl Hamiltonian (68). Equation (76) is in fact very similar to the corresponding expression for the transport collision rate in graphene.[28]

Introducing an effective fine-structure constant $\alpha = e^2/\epsilon_d v_F$, which expresses the ratio of the typical Coulomb interaction energy scale $e^2 k_F/\epsilon_d$ to the typical kinetic energy scale $v_F k_F$ in the Weyl semimetal, Eq. (76) may be written as

$$\frac{1}{\tau_{\rm tr}(\epsilon)} = \frac{\pi \alpha^2 n_i v_F^3}{4\epsilon^2} \int_0^\pi d\theta \frac{\sin^3(\theta)}{[\sin^2(\theta/2) + \alpha/2\pi]^2}. \quad (78)$$

Integrating over the scattering angle, we then obtain the following expression for the transport collision rate:

$$\frac{1}{\tau_{tr}(\epsilon)} = \frac{4\pi^3 n_i v_F^3}{3\epsilon^2} f(\alpha), \quad (79)$$

where

$$f(\alpha) = \frac{3\alpha^2}{\pi^2}\left[(1+\alpha/\pi)\,\text{atanh}\left(\frac{1}{1+\alpha/\pi}\right) - 1\right]. \quad (80)$$

The function $f(\alpha)$ approaches unity for $\alpha \gg 1$, i.e., in the limit of strong interactions and vanishes as

$$f(\alpha) \approx \frac{3\alpha^2}{2\pi^3} \ln(1/\alpha) \quad (81)$$

in the weak interaction $\alpha \ll 1$ limit. If we assume that the charged impurities are donors, i.e., that the impurity concentration is proportional to the electron concentration $n \sim (\epsilon_F/v_F)^3$, then, as obvious from Eq. (79),

$$f(\alpha) \sim \frac{1}{\epsilon_F \tau_{\rm tr}(\epsilon_F)}. \quad (82)$$

The standard Boltzmann-equation expression for the zero-temperature dc conductivity in terms of the transport collision time is given by ($\hbar$ is restored)

$$\sigma_{\rm dc} \sim \frac{e^2 v_F^2}{h} g(\epsilon_F) \tau_{\rm tr}(\epsilon_F). \quad (83)$$

Using Eq. (79) and $n_i \sim (\epsilon_F/v_F)^3$, we finally obtain the following result for the dc conductivity of the Weyl semimetal with Coulomb impurities:

$$\sigma_{\rm dc} \sim \frac{e^2 n_i^{1/3}}{h f(\alpha)}. \quad (84)$$

Scattering from charged impurities thus leads to the dc conductivity vanishing as a function of the dopant concentration as $n_i^{1/3}$. Note that this result can be rewritten in the physically transparent form

$$\sigma_{\rm dc} \sim \frac{e^2}{h} k_F \times (k_F \ell), \quad (85)$$

where the Fermi momentum $k_F \sim n_i^{1/3}$ and $\ell = v_F \tau$ is the mean-free path. This agrees with a simple scaling of conductivity linearly with energy. Moreover, the mean-free path obeys

$$k_F \ell \sim 1/f(\alpha), \quad (86)$$

which implies that electrons are weakly scattered and justifies the semiclassical approximation when $f(\alpha) \ll 1$, i.e., when $\alpha \ll 1$, consistent with the perturbative treatment of scattering.

### 3. *Coulomb scattering at neutrality*

This behavior, however, can not be expected to hold all the way to the neutrality point, and a crossover to a doping-independent value of the conductivity should occur once $\epsilon_F < T$, as happens, e.g., in graphene.[29] In the regime $\epsilon_F < T$, the conductivity can be expected to be determined by scattering due to the (almost) unscreened Coulomb electron-electron interactions (except at higher temperatures, where the short-range scattering from neutral defects, discussed above, will dominate). For the undoped Weyl semimetal at low temperatures, one expects the electron self-energy due to interactions to be proportional to the quasiparticle energy, up to possible multiplicative logarithmic corrections[27]

$$1/\tau \sim \text{Im}\Sigma(\epsilon) \sim \alpha^2 \text{Max}\{\epsilon, T\}. \quad (87)$$

This follows simply from the absence of any energy scales in the undoped Weyl semimetal other than the $\epsilon$ itself, but can also be obtained from an explicit calculation.[27] By interpreting $\text{Im}\Sigma(\epsilon)$ as the scattering rate $1/\tau(\epsilon)$ and plugging it into the Boltzmann-equation expression for the dc conductivity, we obtain

$$\sigma(\omega = n_i = 0) \sim \frac{e^2 v_F^2}{h} \int d\epsilon \left(-\frac{dn_F(\epsilon)}{d\epsilon}\right) g(\epsilon)\tau(\epsilon) \sim \frac{e^2 T}{h\alpha^2 v_F}, \quad (88)$$

i.e., a power-law insulating behavior with the dc conductivity vanishing linearly with temperature.

Note that this form matches nicely the scaling obtained above for the case of donor impurities. In particular, both forms *and* the expected frequency dependence can be encompassed by the general quantum critical scaling form

$$\sigma(\omega, n_i, T) \sim \frac{e^2 k_F}{h\alpha^2} S\left[v_F k_F/T, \omega/T\right], \quad (89)$$

where $S[X,Y]$ is an $O(1)$ scaling function. We have taken the forms appropriate for small $\alpha$, where the perturbative calculations are valid, and neglected logarithms (which are interesting, but beyond the scope of this work). A more detailed study of the conductivity in the absence of donor impurities can be found in a recent preprint.[30]

### B. dc conductivity of the line-node semimetal

Finally, let us discuss transport properties of the line-node semimetal. As will be shown below, these are somewhat similar to graphene,[31–35] except for the fact that they occur in a 3D material. We will also only consider the dc conductivity, as the calculation of the frequency-dependent conductivity is somewhat complicated and in general can only be done numerically (except in the high-frequency limit $\omega\tau \gg 1$). However, as in graphene, we expect the optical conductivity of the line-node semimetal to be only weakly frequency dependent.

For simplicity, we will adopt the model of pointlike randomly distributed impurities, with the potential given by Eq. (67). We assume that only the low-energy states, described by the lower $(-)$ block of the Hamiltonian (37), contribute significantly to transport. The eigenstates of this $2\times 2$ Hamiltonian are given by

$$|\pm,\mathbf{k}\rangle = \frac{1}{\sqrt{2}}(\sqrt{1\pm m(\mathbf{k})/\epsilon(\mathbf{k})}, \mp i\,\mathrm{sign}(k_x)\sqrt{1\mp m(\mathbf{k})/\epsilon(\mathbf{k})}), \tag{90}$$

where $m(\mathbf{k}) \equiv m_-(\mathbf{k}) = b - \sqrt{v_F^2k_y^2+\Delta^2(k_z)}$ and $\epsilon(\mathbf{k}) = \sqrt{v_F^2k_x^2+m^2(\mathbf{k})}$. The corresponding eigenvalues are $\epsilon_\pm(\mathbf{k}) = \pm\epsilon(\mathbf{k})$. Let us first find the low-energy density of states of the nodal line. In general, it can only be calculated numerically. To obtain an analytical expression, we will assume that the size of the nodal line along the $z$ axis is small compared to $\pi/d$. Then, we can expand $\Delta(k_z)$ to leading order in $k_z$ near $k_z = \pi/d$. We obtain

$$\Delta(k_z) \approx \Delta^2 + \tilde{v}_F^2k_z^2, \tag{91}$$

where $\Delta = |\Delta_S - \Delta_D|$ and we have redefined $k_z \to k_z + \pi/d$. The density of states can be most conveniently found by differentiating the function

$$N(\epsilon) = \int \frac{d^3k}{(2\pi)^3}\Theta[\epsilon-\epsilon(\mathbf{k})], \tag{92}$$

where $\Theta(x)$ is the Heaviside theta function. This is proportional to the volume of a torus in momentum space, the surface of which is described by the equation

$$\epsilon^2 = v_F^2k_x^2 + \left[b - \sqrt{v_F^2k_y^2+\tilde{v}_F^2k_z^2+\Delta^2}\right]^2. \tag{93}$$

The cross section of this torus is not circular and its volume in general can not be calculated analytically. An analytical expression can, however, be obtained in the limit $b \gg \Delta$. In this limit, Eq. (93), after appropriate rescaling of the coordinates, describes a canonical torus of major radius $b$ and minor radius $\epsilon$. Then, we obtain

$$N(\epsilon) = \frac{\epsilon^2 b}{4\pi v_F^2\tilde{v}_F}. \tag{94}$$

The density of states is thus given by

$$g(\epsilon) = \frac{dN(\epsilon)}{d\epsilon} = \frac{\epsilon b}{2\pi v_F^2\tilde{v}_F}. \tag{95}$$

The density of states of a 3D nodal line is thus the same (i.e., scales linearly with energy at low energies) as the density of states of point nodes in 2D, as expected. This means that many of the transport properties of the 3D line-node semimetal will be similar to those of graphene. In particular, since the first Born approximation scattering rate $1/\tau(\epsilon) \sim g(\epsilon) \sim \epsilon$, i.e., is of the same order as the quasiparticle energy, the first Born approximation is in fact inapplicable and the self-consistent Born approximation (SCBA) must be used instead. A general SCBA expression for the disorder self-energy is given by

$$\Sigma_\lambda(\mathbf{k},\epsilon) = \sum_{\mathbf{k}',\lambda'}\langle V_{\lambda\lambda'}(\mathbf{k}-\mathbf{k}')V_{\lambda'\lambda}(\mathbf{k}'-\mathbf{k})\rangle G^R_{\lambda'}(\mathbf{k}',\epsilon), \tag{96}$$

where

$$G^R_\lambda(\mathbf{k},\epsilon) = \frac{1}{\epsilon-\epsilon_\lambda(\mathbf{k})-\Sigma_\lambda(\mathbf{k},\epsilon)} \tag{97}$$

is the retarded disorder-averaged Green's function and

$$V_{\lambda\lambda'}(\mathbf{k}-\mathbf{k}') = \langle\lambda,\mathbf{k}|\lambda',\mathbf{k}'\rangle V(\mathbf{k}-\mathbf{k}') \tag{98}$$

is the matrix element of the impurity potential. The angular brackets in Eq. (96) denote impurity averaging. Near the nodal line, we can approximately set $m(\mathbf{k}) \approx 0$, the matrix element in Eq. (96) becomes independent of $\lambda,\lambda'$, and we obtain

$$\Sigma(\epsilon) = \frac{\gamma}{2V}\sum_{\mathbf{k},\lambda} G^R_\lambda(\mathbf{k},\epsilon), \tag{99}$$

i.e., the self-energy is independent of $\mathbf{k}$ and $\lambda$. Since we are interested in $\Sigma(\epsilon)$ at low energies, we can set $\epsilon \to 0$ in Eq. (99). Then, we obtain

$$\Sigma = \gamma\int_{-\infty}^{\infty} g(\epsilon)\frac{\Sigma}{\epsilon^2-\Sigma^2}, \tag{100}$$

where $\Sigma \equiv \Sigma(0)$. Since $g(\epsilon)$ is an even function of the energy, it follows from Eq. (68) that $\Sigma$ is imaginary. By substituting Eq. (95) in (100) and solving the resulting equation, we obtain

$$|\Sigma| \equiv \frac{1}{2\tau} = \epsilon_c e^{-2\pi v_F^2\tilde{v}_F/\gamma b}, \tag{101}$$

where $\epsilon_c$ is the upper cutoff energy, which is of the order of the total bandwidth. Thus, we find that the impurity scattering rate is finite in the zero-energy limit, unlike the naive first Born approximation result. It can, however, be very small in a clean multilayer.

Now, we can evaluate the conductivity. The standard Kubo formula expression reads as

$$\sigma_{\alpha\beta} = \frac{e^2}{\pi}\int_{-\infty}^{\infty} d\epsilon\left(-\frac{dn_F(\epsilon)}{d\epsilon}\right)\int\frac{d^3k}{(2\pi)^3} \times \langle\lambda\mathbf{k}|v_\alpha|\lambda'\mathbf{k}\rangle\langle\lambda'\mathbf{k}|v_\beta|\lambda\mathbf{k}\rangle \mathrm{Im}\,G^R_\lambda(\mathbf{k},\epsilon)\mathrm{Im}\,G^R_{\lambda'}(\mathbf{k},\epsilon), \tag{102}$$

where repeated $\lambda,\lambda'$ indices are summed over. Vertex corrections to Eq. (102) vanish identically. This can be checked by an explicit calculation, but is most easily seen.

Using the $2 \times 2$ momentum-space Hamiltonian

$$\mathcal{H}(\mathbf{k}) = m(\mathbf{k})\sigma^z - v_F k_x \sigma^y, \tag{103}$$

the components of the velocity operator $v_\alpha = \partial\mathcal{H}/\partial k_\alpha$ are given by

$$v_x = -v_F\sigma^y, \quad v_y = -\frac{v_F^2 k_y}{b - m(\mathbf{k})}\sigma^z, \quad v_z = -\frac{\tilde{v}_F^2 k_z}{b - m(\mathbf{k})}\sigma^z, \tag{104}$$

where at low energies we can again use $m(\mathbf{k}) \approx 0$. Matrix elements of the spin operators are given by

$$\begin{aligned}
&\langle +,\mathbf{k}|\sigma^y|+,\mathbf{k}\rangle = -\frac{v_F k_x}{\epsilon(\mathbf{k})}, \quad \langle -,\mathbf{k}|\sigma^y|-,\mathbf{k}\rangle = \frac{v_F k_x}{\epsilon(\mathbf{k})},\\
&\langle +,\mathbf{k}|\sigma^y|-,\mathbf{k}\rangle = \frac{m(\mathbf{k})\hat{k}_x}{\epsilon(\mathbf{k})}, \quad \langle +,\mathbf{k}|\sigma^z|+,\mathbf{k}\rangle = \frac{m(\mathbf{k})}{\epsilon(\mathbf{k})},\\
&\langle -,\mathbf{k}|\sigma^z|-,\mathbf{k}\rangle = -\frac{m(\mathbf{k})}{\epsilon(\mathbf{k})}, \quad \langle +,\mathbf{k}|\sigma^z|-,\mathbf{k}\rangle = \frac{v_F|k_x|}{\epsilon(\mathbf{k})}.
\end{aligned} \tag{105}$$

It follows from Eqs. (104) and (105) that, at low energies, only intraband terms in (102) contribute to $\sigma_{xx}$, while only interband terms contribute to $\sigma_{yy}$ and $\sigma_{zz}$. After a straightforward calculation, we obtain

$$\sigma_{xx} = \sigma_{yy} = \frac{e^2 b}{\pi\tilde{v}_F h}, \quad \sigma_{zz} = \frac{e^2\tilde{v}_F b}{\pi v_F^2 h}, \tag{106}$$

where we have restored explicit $\hbar$. We note here that the vertex corrections to Eq. (102) vanish identically. This can be checked by an explicit calculation, but is most easily seen from the following symmetry of the Hamiltonian (103): $\mathcal{H}(\mathbf{k}) = \mathcal{H}^*(-\mathbf{k})$. It has been shown in Ref. 36 that such a symmetry of the Hamiltonian (combined in our case with the reality of all the matrix elements of the velocity operator) always leads to cancellation of the vertex corrections to conductivity.

The conductivity of the nodal-line semimetal is thus independent of disorder. This is similar to the well-known universality property of the dc conductivity of graphene.[31–35] Unlike in graphene, however, the conductivity of the line-node semimetal does depend on nonuniversal properties of the nodal line, like its perimeter, which is proportional to $b$, and the Fermi velocity. Note that $\sigma_{xx} = \sigma_{yy}$ only in the limit $b \gg \Delta$, i.e., far away from the insulator-semimetal transition. In general, conductivities in all three directions are different. Note that, obviously, an externally applied field will add to the internal exchange field $b$ due to the ordered magnetic impurity moments, leading to a linear dependence of the conductivity on the field. This would be supplemented by an orbital contribution, not discussed here.

The optical conductivity of the line-node semimetal can be expected to behave as a function of frequency in the same way as the optical conductivity of graphene, i.e., to be roughly frequency independent at low frequencies.

As a final note, let us mention the expected behavior of the doped line-node semimetal. As in the case of the Weyl semimetal, discussed above, we will assume that the ionized dopants of density $n_i$ (say donors) act as long-range Coulomb impurity scatterers for the doped carriers. Following the same line of reasoning as in the Weyl semimetal case, we then obtain

$$\sigma \sim \frac{e^2 v_F^2 n_i}{h\,\alpha^2 b^2}, \tag{107}$$

where we have ignored the Fermi velocity anisotropy for simplicity. The conductivity thus scales linearly with the carrier density, the same result as in graphene.[28] This similarity, however, is accidental in this case, as in graphene the linear scaling is obtained in a very different physical situtation: the Coulomb scatterers are charged impurities in the substrate, while the finite carrier density is provided electrically by applying gate voltage.

## VI. DISCUSSION AND CONCLUSIONS

In this paper, we have considered two classes of topological nodal semimetals, both of which occur in a multilayer heterostructure, made of thin TI films, separated by ordinary-insulator spacers. Topologically stable nodes, in which conduction and valence bands touch, occur in this system when TR symmetry is broken, by either magnetic impurities or external magnetic field. Both point- and line-node semimetals are characterized by protected surface states. These are especially robust in the case of the point-node, or Weyl, semimetal. The edge states in this case are chiral quantum Hall edge states, their chiral character making them robust even to hybridization of the bulk Dirac points.[8]

The surface states of the line-node semimetal are "flat bands," i.e., they are approximately dispersionless in a subset of the surface BZ, bounded by a projection of the bulk nodal line onto the surface plane. Since a flat band has a divergent density of states, nontrivial correlation effects, e.g., superconductivity or magnetism, may be expected.[37]

We have discussed transport properties of both types of nodal semimetals, as these can be expected to be important in the experimental characterization of these phases. We summarize those of the Weyl semimetal, including those not derived here, for convenience. If time-reversal symmetry is broken, it may exhibit an anomalous Hall conductivity. A general expression for this is[8]

$$\sigma_{\mu\nu} = \frac{e^2}{h}\epsilon_{\mu\nu\lambda}K_\lambda, \tag{108}$$

where $\mathbf{K}$ is a wave vector, which can be expressed in terms of the Weyl points according to

$$\mathbf{K} = \mathbf{K}_0 + \sum_i q_i \mathbf{k}_i. \tag{109}$$

Here, $q_i = \pm 1$ is the charge [in units of quantized U(1) Berry flux] of the Weyl point located at $\mathbf{k} = \mathbf{k}_i$, and $\mathbf{K}_0$ is a reciprocal lattice vector (which could be zero). The former is a quantized anomalous Hall contribution due to completely filled bands. Note that although Eqs. (108) and (109) generally describe a nonquantized anomalous Hall effect, it can be considered to be "semiquantized" in the sense that if $\mathbf{K}$ is measured experimentally, the universal quantized prefactor $e^2/h$ can be extracted. In our multilayer case, the Hall conductivity is nonzero and semiquantized in this way even in the absence of an applied (orbital) field. In the proposed Weyl semimetal in the

iridium pyrochlores,[6] it vanishes in zero applied field by cubic symmetry. However, an anomalously large Hall coefficient may be induced according to Eqs. (108) and (109), as the Weyl points shift in an applied magnetic field.

In this paper, we showed that the bulk diagonal conductivity in the Weyl semimetal exhibits approximate quantum critical scaling due to Coulomb interactions. This implies that the zero-temperature dc conductivity is proportional to $n_i^{1/3}$, where $n_i$ is the density of charged donor impurities, and that the dependence of the conductivity on temperature and frequency is approximately a universal function of $v_F n_i^{1/3}/T$ and $\omega/T$. We note that this conductivity scaling is a general property of *any* Weyl semimetal, including not only the superlattice structures described here, but also bulk realizations, such as proposed for iridium pyrochlores.[6] A recent preprint draws similar conclusions in a model with $n_i = 0$.[30]

Finally, the diagonal conductivity also gets surface and interface contributions due to edge states. In fact, even in a single crystal, Ising magnetic domains may form, and there can be chiral surface states bound to such a domain wall. In the superlattice model of Sec. III A, this is indeed the case for any domain wall, which is not normal to the $z$ axis. If a sufficient density of such domain walls is present, they may give an appreciable contribution to the diagonal conductivity. In practice, such contributions should be extracted by a careful study of hysteresis and by finding ways to align the magnetic order into a single domain.

Assuming the line node to lie at the Fermi level (which is undoubtedly an approximation as discussed in depth in Sec. IV B 1), the resulting transport properties are somewhat similar to graphene, except for the fact that these occur in a 3D material in our case. This is not unexpected, as a line node in 3D is equivalent to a point node in 2D since a point node can be thought of as a section of the line node by a plane in momentum space. As a consequence, a 3D line node has the same low-energy density of states as a 2D point node, i.e., linear in energy. This, in turn, leads to similarities in the transport properties. In particular, the dc conductivity of the line-node semimetal is "universal" in the sense of being independent of disorder. It is not, however, as universal as the conductivity of graphene, as it does depend on other material parameters, such as Fermi velocities, the magnitude of spin splitting, and the tunneling matrix elements, characterizing the TI and ordinary-insulator layers in the heterostructure.

## ACKNOWLEDGMENTS

We acknowledge useful discussions with C. Xu. Financial support was provided by the NSERC of Canada and a University of Waterloo start-up grant (A.A.B., M.D.H), by NSF Grants No. DMR-0804564 and No. PHY05-51164 (L.B.), and by the Army Research Office through MURI Grant No.W911-NF-09-1-0398 (L.B.). A.A.B. gratefully acknowledges the hospitality of KITP, where part of this work was done.

[1] C. L. Kane and E. J. Mele, Phys. Rev. Lett. **95**, 146802 (2005); B. A. Bernevig, T. L. Hughes, and S.-C. Zhang, Science **314**, 1757 (2006); J. E. Moore and L. Balents, Phys. Rev. B **75**, 121306 (2007); L. Fu, C. L. Kane, and E. J. Mele, Phys. Rev. Lett. **98**, 106803 (2007).

[2] M. König, S. Wiedmann, C. Brüne, A. Roth, H. Buhmann, L. Molenkamp, X.-L. Qi, and S.-C. Zhang, Science **318**, 766 (2007).

[3] Y. Xia, D. Qian, D. Hsieh, L. Wray, A. Pal, H. Lin, A. Bansil, D. Grauer, Y. S. Hor, R. J. Cava, and M. Z. Hasan, Nat. Phys. **5**, 398 (2009).

[4] M. Z. Hasan and C. L. Kane, Rev. Mod. Phys. **82**, 3045 (2010).

[5] X.-L. Qi and S.-C. Zhang, Rev. Mod. Phys. **83**, 1057 (2011).

[6] X. Wan, A. M. Turner, A. Vishwanath, and S. Y. Savrasov, Phys. Rev. B **83**, 205101 (2011).

[7] T. Heikkilä and G. E. Volovik, JETP Lett. **93**, 59 (2011).

[8] K.-Y. Yang, Y.-M. Lu, and Y. Ran, Phys. Rev. B **84**, 075129 (2011).

[9] A. A. Burkov and L. Balents, Phys. Rev. Lett. **107**, 127205 (2011).

[10] W. Witczak-Krempa and Y.-B. Kim, e-print arXiv:1105.6108.

[11] G. Xu, H. Weng, Z. Wang, X. Dai, and Z. Fang, Phys. Rev. Lett. **107**, 186806 (2011).

[12] G. B. Halász and L. Balents, e-print arXiv:1109.6137.

[13] C. Herring, Phys. Rev. **52**, 365 (1937).

[14] G. E. Volovik, *The Universe in a Helium Droplet* (Clarendon, Oxford, 2003).

[15] G. E. Volovik, Lect. Notes Phys. **718**, 31 (2007).

[16] P. Horava, Phys. Rev. Lett. **95**, 016405 (2005).

[17] H. B. Nielsen and N. Ninomiya, Nucl. Phys. B **185**, 20 (1981); **193**, 173 (1981).

[18] S. Murakami, New J. Phys. **9**, 356 (2007).

[19] F. R. Klinkhamer and G. E. Volovik, Int. J. Mod. Phys. A **20**, 2795 (2005).

[20] B. Béri, Phys. Rev. B **81**, 134515 (2010).

[21] R. Jackiw, Phys. Rev. D **29**, 2375 (1984).

[22] G. W. Semenoff, Phys. Rev. Lett. **53**, 2449 (1984).

[23] F. D. M. Haldane, Phys. Rev. Lett. **61**, 2015 (1988).

[24] A. A. Zyuzin and A. A. Burkov, Phys. Rev. B **83**, 195413 (2011).

[25] V. Aji, e-print arXiv:1108.4426.

[26] A. A. Zyuzin, M. D. Hook, and A. A. Burkov, Phys. Rev. B **83**, 245428 (2011).

[27] A. A. Abrikosov and S. D. Beneslavskii, Sov. Phys.–JETP **32**, 699 (1971) [ZhETF **59**, 1280 (1970)].

[28] K. Nomura and A. H. MacDonald, Phys. Rev. Lett. **96**, 256602 (2006).

[29] S. Das Sarma, S. Adam, E. H. Hwang, and E. Rossi, Rev. Mod. Phys. **83**, 407 (2011).

[30] P. Hosur, S. A. Parameswaran, and A. Vishwanath, e-print arXiv:1109.6330.

[31] E. Fradkin, Phys. Rev. B **33**, 3257 (1986).

[32] A. W. W. Ludwig, M. P. A. Fisher, R. Shankar, and G. Grinstein, Phys. Rev. B **50**, 7526 (1994).

[33] N. H. Shon and T. Ando, J. Phys. Soc. Jpn. **67**, 2421 (1998).

[34] V. P. Gusynin and S. G. Sharapov, Phys. Rev. B **73**, 245411 (2006).

[35] N. M. R. Peres, F. Guinea, and A. H. Castro Neto, Phys. Rev. B **73**, 125411 (2006).

[36] S. Murakami, Phys. Rev. B **69**, 241202 (2004).

[37] N. B. Kopnin, T. Heikkilä, and G. E. Volovik, e-print arXiv:1103.2033.